Malaria Sporozoites Traverse Host Cells within Transient Vacuoles

Veronica Risco-Castillo, Selma Topçu, Carine Marinach, Giulia Manzoni, Amélie e. Bigorgne, Sylvie Briquet, Xavier Baudin, Maryse Lebrun, Jean-François Dubremetz, Olivier Silvie

▶ **To cite this version:**

Veronica Risco-Castillo, Selma Topçu, Carine Marinach, Giulia Manzoni, Amélie e. Bigorgne, et al.. Malaria Sporozoites Traverse Host Cells within Transient Vacuoles. Cell Host and Microbe, 2015, 18 (51), pp.593-603. 10.1016/j.chom.2015.10.006 . hal-01226222

HAL Id: hal-01226222

https://hal.sorbonne-universite.fr/hal-01226222v1

Submitted on 9 Nov 2015

HAL is a multi-disciplinary open access archive for the deposit and dissemination of scientific research documents, whether they are published or not. The documents may come from teaching and research institutions in France or abroad, or from public or private research centers.

L'archive ouverte pluridisciplinaire **HAL**, est destinée au dépôt et à la diffusion de documents scientifiques de niveau recherche, publiés ou non, émanant des établissements d'enseignement et de recherche français ou étrangers, des laboratoires publics ou privés.

Malaria sporozoites traverse host cells within transient vacuoles

Veronica Risco-Castillo[1,4#], Selma Topçu[1,4], Carine Marinach[1,4], Giulia Manzoni[1], Amélie E. Bigorgne[1], Sylvie Briquet[1], Xavier Baudin[2], Maryse Lebrun[3], Jean-François Dubremetz[3], Olivier Silvie[1*]

[1]Sorbonne Universités, UPMC Univ Paris 06, INSERM U1135, CNRS ERL8255, Centre d'Immunologie et des Maladies Infectieuses, F-75013, Paris, France.

[2]Sorbonne Paris Cité, Univ Paris Diderot, CNRS, Institut Jacques Monod, ImagoSeine, UMR 7592, Paris F-75205, France

[3]Université de Montpellier 2, CNRS, Dynamique des Interactions Membranaires Normales et Pathologiques, UMR 5235, F-34095 Montpelllier, France.

[4]These authors contributed equally to this work

*Corresponding author:

Centre d'Immunologie et des Maladies Infectieuses

Faculté de Médecine Pierre et Marie Curie

91 Bd de l'Hôpital, 75013 Paris, France

olivier.silvie@inserm.fr

Phone: +33-1-40778111, Fax: +33-1-45838858

#Present address: Ecole Nationale Vétérinaire d'Alfort (EnvA), 94704 Maisons-Alfort, France

Running title: Perforin-dependent egress of malaria sporozoites

Key words: Malaria; *Plasmodium* sporozoites; Perforin-like protein; Cell traversal; Lysosomes

SUMMARY

Plasmodium sporozoites are deposited in the host skin by *Anopheles* mosquitoes. The parasites migrate from the dermis to the liver, where they invade hepatocytes through a moving junction (MJ) to form a replicative parasitophorous vacuole (PV). Malaria sporozoites need to traverse cells during progression through host tissues, a process requiring parasite perforin-like protein 1 (PLP1). We find that sporozoites traverse cells inside transient vacuoles that precede PV formation. Sporozoites initially invade cells inside transient vacuoles by an active MJ-independent process that does not require vacuole membrane remodeling or release of parasite secretory organelles typically involved in invasion. Sporozoites use pH sensing and PLP1 to exit these vacuoles and avoid degradation by host lysosomes. Next, parasites enter the MJ-dependent PV, which has a different membrane composition, precluding lysosome fusion. The malaria parasite has thus evolved different strategies to evade host cell defense and establish an intracellular niche for replication.

INTRODUCTION

Malaria begins when *Plasmodium* sporozoites are deposited in the host skin by a female *Anopheles* mosquito. They rapidly travel to the liver and invade hepatocytes, where they differentiate into exo-erythrocytic forms (EEFs) and pathogenic merozoites inside a membrane-bound compartment, the parasitophorous vacuole (PV). Sporozoite progression through the host tissues following transmission by the mosquito relies on active gliding motility and the capacity of the parasite to migrate through cells (Ménard et al., 2013). During cell traversal (CT), sporozoites breach the host cell membrane and glide through the traversed cell cytoplasm (Mota et al., 2001). Reverse genetics studies have identified several parasite factors involved in sporozoite CT (Bhanot et al., 2005; Ishino et al., 2004, 2005; Kariu et al., 2006; Moreira et al., 2008; Talman et al., 2011). Among these factors, the Perforin-Like Protein 1 (PLP1, also called SPECT2), belongs to an evolutionary conserved family of pore-forming proteins characterized by the presence of a membrane attack complex/perforin (MACPF) domain (Kaiser et al., 2004). Recombinant forms of *P. falciparum* PLP1 protein or its MACPF domain were shown to have membrane lytic activity (Garg et al., 2013). It has been proposed that PLP1-mediated perforation of the host cell plasma membrane facilitates parasite entry into the traversed cell (Ishino et al., 2005), but the mechanisms of membrane rupturing during sporozoite CT have not been elucidated.

The use of CT-deficient mutant *P. berghei* parasites, combined with intravital imaging approaches, established that CT allows migration of the parasites to the liver parenchyma following inoculation by the mosquito. In particular, *plp1*-knockout *P. berghei* sporozoites have reduced infectivity to rodents, associated with a lack of sporozoite CT activity *in vitro* and impaired parasite progression through the dermis and the liver sinusoidal barrier *in vivo* (Amino et al., 2008; Ishino et al., 2005; Tavares et al., 2013). CT was initially proposed to activate the parasite for productive invasion (Mota et al., 2002), notably based on the observation that sporozoites traverse several hepatocytes before establishing a PV, both *in vitro* and *in vivo* (Frevert et al., 2005; Mota et al., 2001). Nevertheless, CT-deficient sporozoites can productively invade hepatocytes *in vitro* as efficiently as WT parasites

(Amino et al., 2008; Ishino et al., 2004, 2005). In one study, *plp1*-deficient *P. berghei* sporozoites were reported to infect cells more rapidly than normal sporozoites, leading to the conclusion that CT retards rather than activates productive invasion (Amino et al., 2008). However, the kinetics of CT and productive invasion during the course of infection have not been studied in detail in any of these studies.

Here we investigated the temporal and molecular mechanisms of CT and productive invasion during sporozoite infection. We found that CT precedes productive invasion, and that during CT *Plasmodium* sporozoites actively invade cells inside transient vacuoles, which are distinct from PVs. *Plp1*-knockout sporozoites fail to egress from transient vacuoles and are eliminated after fusion with the host cell lysosomes. Furthermore, treating cells with a selective inhibitor of lysosomal acidification abrogates sporozoite CT, reproducing the *plp1*-knockout phenotype. Our data reveal that *Plasmodium* sporozoites can actively invade cells inside two different vacuoles, and either use PLP1 and pH sensing to egress from transient non-replicative vacuoles, or remodel the PV membrane to escape degradation by the host cell lysosomal machinery.

RESULTS

Sporozoite host cell traversal precedes productive invasion

To analyze the kinetics of sporozoite CT and host cell infection, we took advantage of a GFP-expressing *P. yoelii* strain (Manzoni et al., 2014) and a robust experimental setup consisting of two related hepatocytic cell lines, HepG2/CD81 and parental HepG2 cells (Silvie et al., 2006a). HepG2/CD81 cells express the host entry factor CD81 and support *P. yoelii* CT and productive invasion, whereas the parental HepG2 cells lack CD81 and support *P. yoelii* CT but not productive invasion (Risco-Castillo et al., 2014; Silvie et al., 2003, 2006a).

CT activity was monitored by flow cytometry using an established wound-repair assay based on uptake of a fluorescent dextran tracer by traversed cells (Mota et al., 2001) (**Figure 1A**). CT activity was maximal during the first hour of sporozoite incubation with cells, as shown by the rapid increase of dextran-positive cell numbers (**Figure 1B**), and was similar in HepG2 and HepG2/CD81 cells, as expected (Silvie et al., 2003, 2006a). The sporozoite invasion rate, defined as the percentage of GFP-positive cells, remained low in HepG2 cells throughout the assay, consistent with the transient intracellular localization of sporozoites during CT (**Figure 1C**). The percentage of GFP-positive HepG2/CD81 cells was also initially low and identical to that in HepG2 cells, and showed a marked increase only after a delay, which varied from 30 to 90 minutes depending on the experiments (**Figure 1C**).

Detection of GFP-positive cells by FACS allows to quantify sporozoite invasion, but does not discriminate between sporozoite CT and productive invasion inside a PV. To distinguish productive from non-productive invasion events, cell cultures inoculated with sporozoites were dissociated by trypsin treatment at different time points, re-plated and cultured for an additional 24-36 hours, before quantification of productive invasion events based on the number of developing EEFs (**Figure 1A**). This assay revealed that early invasion events were non-productive in HepG2/CD81 cells, whereas late invasion events coincided with parasite development into EEFs (**Figure 1D**). Collectively, these data

establish that early invasion events correspond to sporozoite CT activity, and are followed by a second phase of CD81-dependent productive invasion.

Sporozoites form transient vacuoles during cell traversal

Surprisingly, more than 50% of invaded (GFP-positive) HepG2 cells were dextran-negative at early time points, suggestive of parasite entry without membrane damage, whereas later during the course of infection most invaded cells were dextran-positive (**Figure 2A**). Furthermore, transmission electron microscopy (TEM) images of *P. yoelii*-infected HepG2 cells revealed the presence of a membrane around some sporozoites (**Figure 2B-C**). Because *P. yoelii* can traverse but not productively invade HepG2 cells, these results suggest that CT events may involve the formation of transient vacuoles. To test this hypothesis, we imaged PyGFP sporozoites incubated with HepG2 cells expressing a fluorescent marker of the plasma membrane, N20-mCherry, consisting of mCherry fused to the N-terminal region of neuromodulin (Zuber et al., 1989). Shortly after adding sporozoites to HepG2/N20-mCherry cells, intracellular GFP parasites could be observed enclosed in N20-mCherry-labeled vacuoles (**Figure 2D**), which were also stained with filipin, a cholesterol-binding agent that selectively labels the host cell but not the sporozoite membrane (Bano et al., 2007). A large proportion (40-50%) of intracellular sporozoites were contained inside filipin and N20-mCherry-labeled vacuoles at early time points (**Figure 2E**), corroborating the FACS results. In addition, we could image by spinning disk confocal microscopy sporozoite egress from N20-mCherry-labeled vacuoles (**Figure 2F and Movie S1 and S2**). These data provide direct evidence that *Plasmodium* sporozoites can traverse cells by forming transient vacuoles (TVs).

PLP1-deficient sporozoites do not egress from transient vacuoles

We then hypothesized that PLP1, which is required for CT (Ishino et al., 2005), may play a role in egress from TVs. We generated GFP-expressing *plp1*-deficient parasites in *P. yoelii* using the recent ‘Gene Out Marker Out’ strategy (Manzoni et al., 2014) (**Figure S1A**

and S1B). Py∆*plp1* mutants showed no defect during blood stage replication, transmission to mosquitoes and sporozoite production (**Figure S1C-E**). Py∆*plp1* sporozoites were motile and developed into EEFs *in vitro* as efficiently as control parasites, but were poorly infective to mice *in vivo*, especially when administered through mosquito bites, the natural transmission route (**Figure S2A-E**). This loss of infectivity was associated with a complete abrogation of CT activity (**Figure S2F-H**).

Surprisingly, in our *in vitro* invasion assays, the percentage of GFP-positive cells was much higher with Py∆*plp1* sporozoites than with PyGFP, in both HepG2 and HepG2/CD81 cells (**Figure 3A-B,** curves). However, like PyGFP, Py∆*plp1* sporozoites did not develop into EEFs inside HepG2 cells, showing that in the absence of CD81 all invasion events were non-productive (**Figure 3A,** histograms). In HepG2/CD81 cells, Py∆*plp1* formed similar numbers of EEFs as PyGFP (**Figure 3B**, histograms), despite higher invasion rates, indicating that invasion events were for a large part non-productive. EEF development coincided with late invasion events, as observed with PyGFP.

Importantly, all Py∆*plp1* sporozoites inside HepG2 were contained inside a vacuole, as evidenced by TEM (**Figure 3C**) and fluorescent labeling by filipin and N20-mCherry (**Figure 3D and 3E**). No egress of Py∆*plp1* sporozoites was observed in live cell imaging experiments (**Figure 3F** and **Movie S3**). Similar results were obtained with *P. berghei* sporozoites in Hepa1-6 cells (**Figure S3**).

Taken together, these data indicate that PLP1 is required for sporozoite egress from non-replicative TVs but not for entry into cells. Our results also show that abrogation of CT does not accelerate commitment to productive invasion, and that Py∆*plp1* form both TVs and PVs in HepG2/CD81 cells.

TVs are formed without rhoptry secretion or remodeling of the vacuole membrane

Our data show that sporozoites can invade cells inside two types of vacuoles, non-replicative TVs or replicative PVs. We further characterized the mechanism of formation of TVs, using the Py∆*plp1* mutant, where abrogation of sporozoite egress results in the

accumulation of TVs inside cells. PyΔ*plp1* sporozoite invasion of HepG2 and HepG2/CD81 cells was prevented by exposure to cytochalasin D or anti-CSP antibodies, which both inhibit sporozoite motility, (**Figure 4A**). This demonstrates that formation of TVs, like PVs, is an active process driven by the parasite motility, and not the result of passive uptake by the host cells.

We have shown before that productive host cell invasion is associated with discharge of the sporozoite rhoptries, resulting in depletion of the rhoptry proteins RON2 and RON4 (Risco-Castillo et al., 2014). Interestingly, PyΔ*plp1* sporozoite rhoptries, when visible, appeared intact on TEM images of invaded HepG2 cells (**Figure 3C**), suggesting entry without rhoptry secretion. To corroborate this finding, we genetically engineered a PyΔ*plp1* parasite line expressing a mCherry-tagged version of RON4, and examined by fluorescence microscopy RON4-mCherry expression during sporozoite host cell invasion, using filipin staining to label intracellular vacuoles (**Figure 4B**). In HepG2 cells, where all the vacuoles correspond to TVs only, sporozoites still expressed apical RON4-mCherry, at all time points examined, in both PyΔ*plp1*/RON4::mCherry and PyGFP/RON4::mCherry parasites (**Figure 4B and 4C**). In HepG2/CD81 cells, sporozoites inside vacuoles also expressed RON4-mCherry at early time points (30 min), when vacuoles correspond to TVs. Depletion of RON4-mCherry was observed at later time points, indicative of rhoptry discharge during productive invasion and formation of the PVs (**Figure 4B and 4C**). RON4 depletion was seen in a smaller proportion of the PyΔ*plp1*/RON4::mCherry as compared to PyGFP/RON4::mCherry parasites, consistent with the fact that PLP1-deficient sporozoites predominantly form non-productive vacuoles. Altogether, these data confirm that formation of TVs, unlike PVs, occurs without rhoptry discharge.

We next examined the presence of host proteins on the membrane of TVs versus PVs. We found that N20-mCherry and Basigin, an abundant transmembrane protein, were both included in the membrane of PyΔ*plp1* vacuoles inside HepG2 cells, which correspond to TVs (**Figure 4D-F**). Interestingly, a vast majority (>85%) of these vacuoles were also labeled with phalloidin, which binds to F-actin (**Figure 4E and 4F**). Similar results were obtained with

PyGFP sporozoites in HepG2 cells (**Figure S4**). This suggests that sporozoites include cortical cytoskeleton components during formation of TVs. In sharp contrast, all three markers were efficiently excluded from PVs in HepG2/CD81 cells (**Figure 4F-G and Figure S4**). These results indicate that host membrane proteins are excluded from the PV membrane (PVM) during productive invasion, whereas TVs are formed without remodeling of the vacuole membrane.

PyΔ*plp1* non-replicative vacuoles are eliminated by host cell lysosomes

PyΔ*plp1* sporozoites were retained inside vacuoles in HepG2 cells but failed to develop into EEFs, and were eliminated within 12 hours of infection (**Figure 5A**). In HepG2/CD81 cells, the number of infected cells also decreased over time but 20 to 50% of the parasites persisted and developed into EEFs (**Figure 5A**). We hypothesized that the host cell lysosomal machinery may be responsible for the elimination of PyΔ*plp1* non-replicative vacuoles. To test this hypothesis, we used the acidic organelle probe Lysotracker-red and antibodies against the lysosomal associated membrane protein 1 (LAMP1). About 80% of intracellular PyΔ*plp1* parasites were labeled by Lysotracker-red in HepG2 cells, whereas in HepG2/CD81 both Lysotracker-positive and Lysotracker-negative parasites could be found (**Figure 5B and 5D**). Similarly, LAMP1 staining was observed on most PyΔ*plp1* vacuoles inside HepG2 cells, and on a fraction of the parasites inside HepG2/CD81 cells (**Figure 5C and 5D**). Similar results were obtained with *P. berghei* in Hepa1-6 cells (**Figure S3F**).

To further explore whether a similar phenomenon occurs *in vivo*, we examined liver cryosections from BALB/c mice injected with PyGFP or PyΔ*plp1* sporozoites. PyΔ*plp1* parasites detected in the liver parenchyma lacked the PVM marker UIS4 but were labeled by anti-LAMP1 antibodies (**Figure 5E** and **Figure S5A-B**), corroborating results obtained in cell cultures (**Figure 5D** and **Figure S5C-D**). Conversely, only a minority of PyGFP parasites was LAMP1-positive in the liver, showing that a large proportion of WT parasites do not fuse with lysosomes in infected hepatocytes *in vivo*.

We also documented the degradation of non-replicative PyΔ*plp1* vacuoles by TEM analysis of infected HepG2 cells, which revealed accumulation of granular material inside the vacuole, suggestive of secondary lysosomes (**Figure S5E**).

Treatment of cells with chloroquine (CQ), to inhibit lysosome acidification, enhanced PyΔ*plp1* sporozoite persistence in HepG2 cells (**Figure 5F**), but these sporozoites still failed to develop into EEFs (data not shown). Collectively, our results reveal that invaded PyΔ*plp1* parasites are efficiently recognized and eliminated by the host cell lysosomes in HepG2 cells, whereas in HepG2/CD81 cells some parasites successfully form a PV, via CD81, avoid lysosomal degradation and develop into EEFs. Accordingly, PyGFP and PyΔ*plp1* EEFs developing inside HepG2/CD81 cells were not labeled by Lysotracker-red (**Figure S5F**).

PLP1-mediated sporozoite egress depends on lysosomal acidification

In *T. gondii*, low pH promotes membrane binding and cytolytic activity of PLP1 (Roiko et al., 2014). We hypothesized that *Plasmodium* PLP1 activity might also be regulated by the pH, and that acidification of the vacuole upon fusion with lysosomes would activate PLP1 and parasite egress from TVs. To test this hypothesis, we incubated PyGFP sporozoites with host cells pre-treated with bafilomycin A1, a selective inhibitor of vacuolar-type H^+-ATPases that blocks lysosomal acidification (Yoshimori et al., 1991). Remarkably, pre-treatment of cells with bafilomycin A1 suppressed sporozoite CT (**Figure 6A-B**). Concomitantly, we observed an increase in the number of PyGFP-invaded cells, in both HepG2/CD81 cells and HepG2 cells (**Figure 6A-B**, red bars). These results are reminiscent of the behavior of PyΔ*plp1* sporozoites (**Figure 3 A-B**). Similar numbers of EEFs were observed in bafilomycin A1-treated cells as in control cells (**Figure 6C**). However, in addition to EEFs, a population of non-developing sporozoites was observed in bafilomycin A1 treated cells (**Figure 6D**). These persisting intracellular sporozoites were found in both HepG2 and HepG2/CD81, and likely correspond to parasites that did not egress from non-replicative TVs yet avoided degradation owing to inhibition of lysosome function, as observed with PyΔ*plp1* mutant parasites in CQ-treated cells.

Collectively, our data support a model where *Plasmodium* sporozoites, during CT, actively invade cells inside transient non-replicative vacuoles, independently of host entry factors and without forming a moving junction (**Figure 7**). Sporozoites use pH sensing and PLP1 to egress from these non-replicative vacuoles and avoid degradation by the host cell lysosomal machinery. Subsequently, parasites enter a MJ-dependent PV that supports parasite liver stage development.

DISCUSSION

Malaria sporozoites can invade cells either transiently during CT, or by establishing a resident PV where they further develop into EEFs. Here we show that transmigrating sporozoites do not necessarily breach the host cell membrane at the time of invasion, as currently believed, but enter cells inside transient vacuoles, from which they subsequently egress using PLP1 and pH sensing. Our FACS and microscopy data demonstrate that a large proportion of early CT events occur after the formation of TVs, whereas late traversal events are associated with membrane rupture before complete sealing of a primary vacuole. This might be due to variations in parasite motility over time or reflect the timing of secretion and/or activation of PLP1.

Apicomplexan zoites productively invade host cells through a MJ, a structure composed in part by RON proteins secreted from the parasite rhoptries (Besteiro et al., 2011). The MJ anchors the invading parasite to the host cell, and serves as a molecular sieve that selectively excludes host proteins from the membrane of the nascent vacuole, resulting in protection from the host cell lysosomes (Mordue et al., 1999). Although the nature of the *Plasmodium* sporozoite MJ remains elusive, our data show that productive invasion is associated with depletion of sporozoite RON proteins and exclusion of several host proteins from the PVM. In contrast, we observed no sign of depletion of RON4 from sporozoites during formation of TVs. Although we cannot formally exclude partial rhoptry secretion during non-productive invasion, these results, combined with the TEM images, strongly suggest that rhoptries are not discharged during entry inside TVs. In addition, we provide evidence that host membrane proteins as well as cortical F-actin are incorporated in the membrane of TVs. This suggests that molecular partitioning occurs during productive invasion only, supposedly at the moving junction, but not during TV formation. Collectively, our data illustrate that TVs are formed without rhoptry secretion or remodeling of the vacuole membrane, two characteristic features of MJ-dependent productive invasion. From these data we conclude that formation of TVs results from active MJ-independent sporozoite invasion, which is different from the classical mechanism of PV formation in Apicomplexa.

Analysis of the invasion kinetics of PyGFP and PyΔ*plp1* sporozoites indicates that most non-productive events occur earlier than productive host cell entry. This observation suggests that vigorous sporozoite motility allows parasite internalization inside TVs, whereas productive invasion inside the PV is only possible after activation of the parasite. It has been proposed that CT activates sporozoites for commitment to productive invasion (Mota et al., 2002). However, CT-deficient *P. berghei* (Ishino et al., 2004, 2005) and *P. yoelii* (this study) sporozoites infect hepatocytes with normal efficiency *in vitro*, showing that prior contact with the host cell cytoplasm is not required for parasite activation. Another study reported that CT retards productive invasion, based on the observation that PbΔ*plp1* sporozoites invade cells more rapidly than normal parasites (Amino et al., 2008). We also observed that PyΔ*plp1* and PbΔ*plp1* sporozoites invade cells more rapidly than control parasites, yet our data clearly show that these early events are non-productive. Productive invasion occurs after a significant delay in both WT and CT-deficient parasites, indicating that CT itself has no impact on parasite activation. The delayed onset of productive invasion that we observed *in vitro* is consistent with the physiological need for the parasite to migrate from the injection site in the skin to its replication site in the liver *in vivo*. In this regard, it has been shown that *P. yoelii* sporozoites leave the inoculation site in the skin up to one hour or more after intradermal injection (Yamauchi et al., 2007).

PLP1-deficient sporozoites, similarly to WT parasites, invade cells by forming TVs but fail to egress and are retained inside non-replicative vacuoles that fuse with lysosomes, resulting in a dramatic reduction of infectivity *in vivo*. Not surprisingly, they remain capable of forming EEFs *in vitro*, as observed before with CT-deficient *P. berghei* lines (Bhanot et al., 2005; Ishino et al., 2004, 2005; Kariu et al., 2006; Moreira et al., 2008; Talman et al., 2011). It should be noted that *in vitro* only a small proportion (less than 10%) of the PyΔ*plp1* sporozoites invade cells and get trapped inside TVs during the early stages of infection. Most parasites remain extracellular and can eventually commit to the second phase of productive invasion upon activation, explaining why EEF numbers are not reduced *in vitro* with the Δ*plp1* mutants. Alternatively, we cannot exclude that some sporozoites may also form a

junction post-invasion, from within a primary non-replicative vacuole, to form a secondary replicative PV (**Figure 7**). In such a scenario, the MJ may serve primarily for molecular partitioning, to modify the vacuole membrane and avoid its recognition by the host cell lysosomes. Along this line, a recent study showed that *T. gondii* tachyzoites internalized inside macrophages by phagocytosis can then actively invade from within the phagosomal compartment to form a PV (Zhao et al., 2014).

We uncovered here a role for PLP1 in sporozoite egress from TVs during CT, revealing that parasite egress and cell traversal are intricate mechanisms. Many pathogens use pore-forming proteins to disrupt host membranes during infection, including for escaping from vacuolar compartments. For example, *Listeria monocytogenes* uses the pore-forming toxin Listeriolysin O (LLO) to egress from phagolysosomes and reach the infected cell cytosol to replicate (Hamon et al., 2012). Several apicomplexan PLPs are implicated in parasite egress events. *Plasmodium* PLP2 was recently shown to play a role in permeabilizing the erythrocyte membrane during egress of *P. falciparum* and *P. berghei* gametocytes (Deligianni et al., 2013; Wirth et al., 2014). PLP1 was reported to play a role in egress of *P. falciparum* merozoites from infected erythrocytes (Garg et al., 2013). Intriguingly, previous proteomic studies in *P. falciparum* have detected PLP1 at the sporozoite stage only (PlasmoDB.org), and PLP1-deficient *P. berghei* and *P. yoelii* parasites show no defect during erythrocytic growth, ruling out any important role of PLP1 during the blood stages, at least in rodent malaria parasites. In *T. gondii*, TgPLP1 mediates the rapid egress of tachyzoites from the host cell after parasite replication, and is involved in the permeabilization of both the PVM and the host cell membrane (Kafsack et al., 2009).

Sporozoites must switch off their CT machinery once they have invaded a cell by forming a PV, to avoid the rupture of the PVM. This may be achieved through control of PLP1 secretion from the micronemes and/or through regulation of the protein activity. Here we show that treating cells with bafilomycin A1, an inhibitor of lysosomal acidification, suppresses sporozoite egress from TVs and cell traversal. This reveals that the parasite uses pH sensing to activate PLP1-dependent egress and avoid degradation by the host cell

lysosomal machinery. Proteins with MACPF domains are typically secreted as monomers, bind to their target membrane, oligomerize, then undergo a conformational change that leads to the formation of a pore (Dunstone and Tweten, 2012). Various pore-forming proteins are regulated by the pH, including *Listeria* LLO and *Toxoplasma* PLP1 (Roiko et al., 2014; Schuerch et al., 2005). Although the mechanism underlying *Plasmodium* PLP1 regulation by pH remains to be defined, our data support a model where *Plasmodium* sporozoites use pH sensing to detect the fusion of the vacuole with the lysosomes, activate PLP1 and egress from the vacuole. During productive invasion, modification of the PVM by molecular partitioning at the moving junction precludes its fusion with the host cell lysosomes, preventing activation of PLP1 and egress from the PV. Alternatively, remodeling of the PVM during parasite entry may alter the binding properties of PLP1 and render the PVM refractory to PLP1 lytic activity.

In conclusion, this study provides insights into temporal and molecular mechanisms of cell traversal versus productive invasion during the early stages of malaria. Our data reveal that *Plasmodium* sporozoites actively invade cells inside two types of vacuoles, and use two different strategies, egress from the vacuole or remodeling of the vacuole membrane, to escape degradation by the host cell lysosomes. These findings illustrate how the malaria parasite evades the host cell defense mechanisms to ensure its safe migration from the skin to the liver and the establishment of a suitable intracellular niche for replication.

EXPERIMENTAL PROCEDURES

Experimental animals and ethics statement

Female Swiss and BALB/c mice (6–8 weeks old, from Janvier) were used for parasite infections. All animal work was conducted in strict accordance with the Directive 2010/63/EU of the European Parliament and Council 'On the protection of animals used for scientific purposes'. The protocol was approved by the Charles Darwin Ethics Committee of the University Pierre et Marie Curie, Paris, France (permit number Ce5/2012/001).

Parasites and cell lines

We used reference *P. yoelii* 17XNL (clone 1.1) and *P. berghei* ANKA (clone 15cy1) parasites. Control GFP-expressing PyGFP and PbGFP parasite lines (Manzoni et al., 2014) were obtained after integration of a GFP expression cassette at the dispensable *P230p* locus. *Anopheles stephensi* mosquitoes were fed on *P. yoelii* or *P. berghei*-infected mice using standard methods (Ramakrishnan et al., 2013), and kept at 24°C and 21°C, respectively. *P. yoelii* and *P. berghei* sporozoites were collected from the salivary glands of infected mosquitoes 14-18 or 21-28 days post-feeding, respectively. Hepatoma cell lines were cultured at 37°C under 5% CO_2 in DMEM supplemented with 10% fetal calf serum and antibiotics (Life Technologies), as described (Silvie et al., 2007). Stable expression of mCherry fused to the N-terminal 20 amino acids of neuromodulin (N20-mCherry) was achieved by cell transduction with a lentiviral vector (Vectalys), following the manufacturer's instructions.

Targeted *PLP1* gene deletion in *P. yoelii* and *P. berghei*

Py*Δplp1* and Pb*Δplp1* mutant parasites were generated using a 'Gene Out Marker Out' strategy (Manzoni et al., 2014). *P. yoelii* 17XNL and *P. berghei* ANKA WT parasites were transfected with *pyplp1* and *pbplp1* targeting constructs, respectively, using standard transfection methods (Janse et al., 2006). GFP-expressing parasite mutants were isolated by flow cytometry after positive and negative selection rounds, as described (Manzoni et al.,

2014). Correct construct integration was confirmed by analytical PCR using specific primer combinations. For mCherry tagging of *P. yoelii* RON4, drug-selectable marker-free Py*Δplp1* parasites were transfected with a PyRON4 targeting vector, as described (Risco-Castillo et al., 2014), and recombinant parasites were isolated by flow cytometry. Details on construct design and parasite transfections are provided as Supplemental Experimental Procedures.

Sporozoite cell traversal and invasion assays

Sporozoite CT and invasion were monitored by flow cytometry (Prudêncio et al., 2008). Briefly, hepatoma cells (5 x 10^4 per well in collagen-coated 96-well plates) were incubated with GFP-expressing sporozoites (5 x 10^3 to 3 x 10^4 per well) in the presence of 0.5 mg/ml rhodamine-conjugated dextran (Life technologies). At different time points, cell cultures were washed, trypsinized and analyzed on a Guava EasyCyte 6/2L bench cytometer equipped with 488 and 532 nm lasers (Millipore), for detection of GFP-positive and dextran-positive cells. For inhibition of lysosome acidification, cells were treated with 1 µM bafilomycin A1 or 100 µM chloroquine (Sigma) for 2 or 12 hours, respectively, or with the solvent alone (DMSO) as a control. Cultures were washed before addition of sporozoites. In some experiments, invasion assays were performed in the presence of 10 µg/ml NYS1 anti-CSP antibody (Charoenvit et al., 1987), 25 µg/ml MT81 anti-CD81 antibody (Silvie et al., 2006b) or 1 µg/ml cytochalasin D (Sigma). To study the kinetics of productive invasion events, sporozoite-infected cell cultures were trypsinized at different time points, replated in 96-well plates and further cultured for 24-36 hours. Cells were then fixed with 4% PFA and the number of EEFs was determined by fluorescence microscopy.

Fluorescence microscopy

For imaging experiments, cells were plated in Ibidi 96-well µ-plates (Biovalley), and imaged on a Zeiss Axio Observer.Z1 inverted fluorescence microscope equipped with LD Plan-Neofluar 40X/0.6 Corr Ph2 M27 and Plan-Apochromat 63X/1.40 Oil DIC M27 objectives. Images acquired using the Zen 2012 software (Zeiss) were processed with ImageJ or

Photoshop CS6 software (Adobe) for adjustment of contrast. To assess liver stage development, HepG2/CD81 cells were infected with *P. yoelii* WT, PyGFP or Py*Δplp1* sporozoites and cultured for 6 to 36 hours before fixation with 4% PFA. Cells were then permeabilized with Triton X-100, and the parasites were stained using antibodies specific for *Plasmodium* HSP70 (Tsuji et al., 1994) and UIS4 (Sicgen). Nuclei were stained with Hoechst 33342 (Life Technologies). For visualization of cell membranes, infected cultures were fixed with 4% PFA and labeled with filipin (Sigma), phalloidin-TRITC (Sigma), and/or anti-basigin antibodies (8A6, Abcam). For quantitative analysis, at least 40 parasites were examined per condition. For lysosome visualization, hepatoma cells infected with GFP-expressing sporozoites were incubated with 60 nM Lysotracker Red DND-99 (Life Technologies) for 30 min before fluorescence microscopy imaging. LAMP1 immunostaining was performed on fixed cells, using monoclonal antibodies specific for human (H4A3, Abcam) or mouse (1D4B, Abcam) LAMP1. For immunostaining of mouse liver sections, BALB/c mice were injected in the tail vein with 1 x 10^6 PyGFP or Py*Δplp1* sporozoites, and euthanized three hours later. The liver was removed, immediately frozen in liquid nitrogen and cut into 7 µm cryosections. Liver sections were fixed in 4% paraformaldehyde, permeabilized in 1% Triton X100 and analyzed by immunofluorescence using antibodies against mouse LAMP1 (1D4B, Abcam) and parasite CSP (Charoenvit et al., 1987).

Spinning disk confocal microscopy

HepG2 cells expressing the N20-mCherry membrane marker were plated in Ibidi 8-well µ-slides (Biovalley). After addition of PyGFP or Py*Δplp1* sporozoites, cultures were placed onto a spinning disk microscope system in a controlled chamber at 37°C under 5% CO_2. We used a CSU22 spinning-disk confocal system (Yokogawa) mounted on a DMI 6000 inverted microscope (Leica), equipped with a Plan-Apochromat 100X/1.40 Oil objective and a cooled EMCCD camera QuantEM 512SC (Photometrics), and driven by Metamorph 7 software (Molecular Devices). Images were recorded every 5 seconds during 15 min, and processed with ImageJ for adjustment of contrast.

Transmission Electron Microscopy

HepG2 cell cultures were incubated with PyΔ*plp1* sporozoites for 45 min or 5 hours before fixation with 2.5% glutaraldehyde in 0.15 M cacodylate buffer. Samples were then treated with 1% osmium tetroxide, dehydrated in a series of ethanol concentrations, and embedded in EPON resin mixture. Ultrathin sections (50 to 60 nm) were observed with a Jeol 1200EXII (Tokio, Japon) transmission electron microscope. Images were recorded with a Quemesa 11 Mpixel camera and the iTEM software (Olympus Soft Imaging Solutions, Munster, Germany).

Statistical analysis

Statistical significance was assessed by non-parametric analysis using the Mann-Whitney U, Kruskal–Wallis and log rank (Mantel-Cox) tests. Multiple comparisons were performed by two-way ANOVA followed by Bonferroni post-test. All statistical tests were computed with GraphPad Prism 5 (GraphPad Software). *In vitro* experiments were performed at least three times, with a minimum of three technical replicates per experiment. *In vivo* experiments in mice were only performed once or twice, as indicated, to minimize animal usage.

AUTHOR CONTRIBUTIONS

V.R.C., S.T. and C.M. designed and performed experiments and analyzed the data; G.M., A.E.B. and S.B. performed experiments; X.B. performed spinning disk microscopy; M.L. analyzed the data; J.F.D. performed electron microscopy and analyzed the data; O.S. supervised the project, designed experiments and analyzed the data, and wrote the manuscript with contributions from all authors.

ACKNOWLEDGMENTS

We thank Jean-François Franetich, Maurel Tefit, Thierry Houpert and Sylvie Minard for rearing the mosquitoes; Bénédicte Hoareau-Coudert (Flow Cytometry Core CyPS) for parasite sorting by flow cytometry; Julius Hafalla and Arnaud Moris for helpful discussions. We acknowledge the ImagoSeine facility, member of the France BioImaging infrastructure supported by the Agence Nationale de la Recherche (ANR-10-INSB-04). This work was funded by the European Union (FP7 Marie Curie grant PCIG10-GA-2011-304081, FP7 PathCo Collaborative Project HEALTH-F3-2012-305578), the Agence Nationale de la Recherche (ANR-10-PDOC-008-01) and the Laboratoire d'Excellence ParaFrap (ANR-11-LABX-0024). GM was supported by a “DIM Malinf” doctoral fellowship awarded by the Conseil Régional d'Ile-de-France.

REFERENCES

Amino, R., Giovannini, D., Thiberge, S., Gueirard, P., Boisson, B., Dubremetz, J.-F., Prévost, M.-C., Ishino, T., Yuda, M., and Ménard, R. (2008). Host cell traversal is important for progression of the malaria parasite through the dermis to the liver. Cell Host Microbe *3*, 88–96.

Bano, N., Romano, J.D., Jayabalasingham, B., and Coppens, I. (2007). Cellular interactions of Plasmodium liver stage with its host mammalian cell. Int J Parasitol *37*, 1329–1341.

Besteiro, S., Dubremetz, J.F., and Lebrun, M. (2011). The moving junction of apicomplexan parasites: a key structure for invasion. Cell Microbiol *13*, 797–805.

Bhanot, P., Schauer, K., Coppens, I., and Nussenzweig, V. (2005). A surface phospholipase is involved in the migration of plasmodium sporozoites through cells. J Biol Chem *280*, 6752–6760.

Charoenvit, Y., Leef, M.F., Yuan, L.F., Sedegah, M., and Beaudoin, R.L. (1987). Characterization of Plasmodium yoelii monoclonal antibodies directed against stage-specific sporozoite antigens. Infect. Immun. *55*, 604–608.

Deligianni, E., Morgan, R.N., Bertuccini, L., Wirth, C.C., Silmon de Monerri, N.C., Spanos, L., Blackman, M.J., Louis, C., Pradel, G., and Siden-Kiamos, I. (2013). A perforin-like protein mediates disruption of the erythrocyte membrane during egress of Plasmodium berghei male gametocytes. Cell. Microbiol. *15*, 1438–1455.

Dunstone, M.A., and Tweten, R.K. (2012). Packing a punch : the mechanism of pore formation by cholesterol dependent cytolysins and membrane attack complex / perforin-like proteins. Curr. Opin. Struct. Biol. *22*, 342–349.

Frevert, U., Engelmann, S., Zougbede, S., Stange, J., Ng, B., Matuschewski, K., Liebes, L., and Yee, H. (2005). Intravital observation of Plasmodium berghei sporozoite infection of the liver. PLoS Biol *3*, e192.

Garg, S., Agarwal, S., Kumar, S., Yazdani, S.S., Chitnis, C.E., and Singh, S. (2013). Calcium-dependent permeabilization of erythrocytes by a perforin-like protein during egress of malaria parasites. Nat. Commun. *4*, 1736.

Hamon, M.A., Ribet, D., Stavru, F., and Cossart, P. (2012). Listeriolysin O: The Swiss army knife of Listeria. Trends Microbiol. *20*, 360–368.

Ishino, T., Yano, K., Chinzei, Y., and Yuda, M. (2004). Cell-passage activity is required for the malarial parasite to cross the liver sinusoidal cell layer. PLoS Biol *2*, E4.

Ishino, T., Chinzei, Y., and Yuda, M. (2005). A Plasmodium sporozoite protein with a membrane attack complex domain is required for breaching the liver sinusoidal cell layer prior to hepatocyte infection. Cell Microbiol *7*, 199–208.

Janse, C.J., Ramesar, J., and Waters, A.P. (2006). High-efficiency transfection and drug selection of genetically transformed blood stages of the rodent malaria parasite Plasmodium berghei. Nat Protoc *1*, 346–356.

Kafsack, B.F.C., Pena, J.D.O., Coppens, I., Ravindran, S., Boothroyd, J.C., and Carruthers, V.B. (2009). Rapid membrane disruption by a perforin-like protein facilitates parasite exit from host cells. Science *323*, 530–533.

Kaiser, K., Camargo, N., Coppens, I., Morrisey, J.M., Vaidya, A.B., and Kappe, S.H. (2004). A member of a conserved Plasmodium protein family with membrane-attack complex/perforin (MACPF)-like domains localizes to the micronemes of sporozoites. Mol Biochem Parasitol *133*, 15–26.

Kariu, T., Ishino, T., Yano, K., Chinzei, Y., and Yuda, M. (2006). CelTOS, a novel malarial protein that mediates transmission to mosquito and vertebrate hosts. Mol Microbiol *59*, 1369–1379.

Manzoni, G., Briquet, S., Risco-Castillo, V., Gaultier, C., Topcu, S., Ivanescu, M.L., Franetich, J.F., Hoareau-Coudert, B., Mazier, D., and Silvie, O. (2014). A rapid and robust selection procedure for generating drug-selectable marker-free recombinant malaria parasites. Sci Rep *4*, 4760.

Ménard, R., Tavares, J., Cockburn, I., Markus, M., Zavala, F., and Amino, R. (2013). Looking under the skin: the first steps in malarial infection and immunity. Nat Rev Microbiol *11*, 701–712.

Mordue, D.G., Desai, N., Dustin, M., and Sibley, L.D. (1999). Invasion by Toxoplasma gondii establishes a moving junction that selectively excludes host cell plasma membrane proteins on the basis of their membrane anchoring. J Exp Med *190*, 1783–1792.

Moreira, C.K., Templeton, T.J., Lavazec, C., Hayward, R.E., Hobbs, C. V, Kroeze, H., Janse, C.J., Waters, A.P., Sinnis, P., and Coppi, A. (2008). The Plasmodium TRAP / MIC2 family member , TRAP-Like Protein (TLP), is involved in tissue traversal by sporozoites. *10*, 1505–1516.

Mota, M.M., Pradel, G., Vanderberg, J.P., Hafalla, J.C., Frevert, U., Nussenzweig, R.S., Nussenzweig, V., and Rodriguez, A. (2001). Migration of Plasmodium sporozoites through cells before infection. Science *291*, 141–144.

Mota, M.M., Hafalla, J.C., and Rodriguez, A. (2002). Migration through host cells activates Plasmodium sporozoites for infection. Nat Med *8*, 1318–1322.

Prudêncio, M., Rodrigues, C.D., Ataíde, R., and Mota, M.M. (2008). Dissecting in vitro host cell infection by Plasmodium sporozoites using flow cytometry. Cell. Microbiol. *10*, 218–224.

Ramakrishnan, C., Delves, M.J., Lal, K., Blagborough, A.M., Butcher, G., Baker, K.W., and Sinden, R.E. (2013). Laboratory maintenance of rodent malaria parasites. Methods Mol Biol *923*, 51–72.

Risco-Castillo, V., Topcu, S., Son, O., Briquet, S., Manzoni, G., and Silvie, O. (2014). CD81 is required for rhoptry discharge during host cell invasion by Plasmodium yoelii sporozoites. Cell Microbiol *16*, 1533–1548.

Roiko, M.S., Svezhova, N., and Carruthers, V.B. (2014). Acidification Activates Toxoplasma gondii Motility and Egress by Enhancing Protein Secretion and Cytolytic Activity. PLoS Pathog. *10*, e1004488.

Schuerch, D.W., Wilson-Kubalek, E.M., and Tweten, R.K. (2005). Molecular basis of listeriolysin O pH dependence. Proc. Natl. Acad. Sci. U. S. A. *102*, 12537–12542.

Silvie, O., Rubinstein, E., Franetich, J.-F., Prenant, M., Belnoue, E., Rénia, L., Hannoun, L., Eling, W., Levy, S., Boucheix, C., et al. (2003). Hepatocyte CD81 is required for Plasmodium falciparum and Plasmodium yoelii sporozoite infectivity. Nat. Med. *9*, 93–96.

Silvie, O., Greco, C., Franetich, J.F., Dubart-Kupperschmitt, A., Hannoun, L., van Gemert, G.J., Sauerwein, R.W., Levy, S., Boucheix, C., Rubinstein, E., et al. (2006a). Expression of human CD81 differently affects host cell susceptibility to malaria sporozoites depending on the Plasmodium species. Cell Microbiol *8*, 1134–1146.

Silvie, O., Charrin, S., Billard, M., Franetich, J.F., Clark, K.L., van Gemert, G.J., Sauerwein, R.W., Dautry, F., Boucheix, C., Mazier, D., et al. (2006b). Cholesterol contributes to the organization of tetraspanin-enriched microdomains and to CD81-dependent infection by malaria sporozoites. J Cell Sci *119*, 1992–2002.

Silvie, O., Franetich, J.F., Boucheix, C., Rubinstein, E., and Mazier, D. (2007). Alternative invasion pathways for Plasmodium berghei sporozoites. Int J Parasitol *37*, 173–182.

Talman, A.M., Lacroix, C., Marques, S.R., Blagborough, A.M., Carzaniga, R., Ménard, R., and Sinden, R.E. (2011). PbGEST mediates malaria transmission to both mosquito and vertebrate host. Mol. Microbiol. *82*, 462–474.

Tavares, J., Formaglio, P., Thiberge, S., Mordelet, E., Van Rooijen, N., Medvinsky, A., Ménard, R., and Amino, R. (2013). Role of host cell traversal by the malaria sporozoite during liver infection. J. Exp. Med. *210*, 905–915.

Tsuji, M., Mattei, D., Nussenzweig, R.S., Eichinger, D., and Zavala, F. (1994). Demonstration of heat-shock protein 70 in the sporozoite stage of malaria parasites. Parasitol. Res. *80*, 16–21.

Wirth, C.C., Glushakova, S., Scheuermayer, M., Repnik, U., Garg, S., Schaack, D., Kachman, M.M., Weißbach, T., Zimmerberg, J., Dandekar, T., et al. (2014). Perforin-like protein PPLP2 permeabilizes the red blood cell membrane during egress of Plasmodium falciparum gametocytes. Cell. Microbiol. *16*, 709–733.

Yamauchi, L.M., Coppi, A., Snounou, G., and Sinnis, P. (2007). Plasmodium sporozoites trickle out of the injection site. Cell. Microbiol. *9*, 1215–1222.

Yoshimori, T., Yamamoto, A., Moriyama, Y., Futai, M., and Tashiro, Y. (1991). Bafilomycin A1, a specific inhibitor of vacuolar-type H(+)-ATPase, inhibits acidification and protein degradation in lysosomes of cultured cells. J. Biol. Chem. *266*, 17707–17712.

Zhao, Y., Marple, A.H., Ferguson, D.J.P., Bzik, D.J., and Yap, G.S. (2014). Avirulent strains of Toxoplasma gondii infect macrophages by active invasion from the phagosome. Proc. Natl. Acad. Sci. U. S. A. *111*, 6437–6442.

Zuber, M.X., Strittmatter, S.M., and Fishman, M.C. (1989). A membrane-targeting signal in the amino terminus of the neuronal protein GAP-43. Nature *341*, 345–348.

FIGURE LEGENDS

Figure 1. Kinetics of *P. yoelii* cell traversal and cell invasion. A. Invasion/infection assay. Cell cultures were incubated for 10 to 180 min with GFP-expressing sporozoites in the presence of rhodamine-labeled dextran, trypsinized and either directly analyzed by FACS, to determine the percentage of traversed (dextran-positive) and invaded (GFP-positive) cells, or replated and further incubated for 24 to 48 h, to determine the number of EEF-infected cells by fluorescence microscopy (productive infection). B-C. HepG2 and HepG2/CD81 cells (5 x 10^4) were incubated at 37°C with PyGFP sporozoites (3 x 10^4) in the presence of rhodamine-conjugated dextran, and analyzed by FACS to determine the percentage of traversed (dextran-positive) cells (B) and invaded (GFP-positive) cells (C). Results are expressed as the mean percentage (+/- SD) of triplicate wells. Statistical significance was assessed using two-way ANOVA followed by Bonferroni test. *** $p<0.001$. D. HepG2/CD81 cell cultures were incubated with PyGFP sporozoites for 10 to 120 minutes, dissociated and replated and cultured for an additional 24 hours, to determine the number of EEFs by fluorescence microscopy.

Figure 2. Sporozoites form transient vacuoles during cell traversal. A. HepG2 cells were incubated with PyGFP sporozoites in the presence of rhodamine-labeled dextran for 15 or 120 minutes. Cells were then trypsinized and analyzed by FACS to determine the proportion of dextran-negative cells among infected (GFP-positive) cells. B-C. Electron micrographs of PyGFP sporozoites inside HepG2 cells, 1 hour post-infection. A vacuole membrane surrounds the parasite in B but not in C. The insets show at higher magnification the parasite plasma membrane (arrow) and the vacuole membrane (arrowheads). Rhoptries are indicated with asterisks. Bars, 2 µm. D. HepG2 cells expressing the fluorescent plasma membrane protein N20-mCherry (red) were incubated with PyGFP sporozoites (green) for 30 min, fixed and labeled with filipin (blue). Bars, 10 µm. E. HepG2/N20-mCherry cells were incubated with PyGFP sporozoites for 30 or 120 min before fixation and labeling with filipin, and the presence or absence of a vacuole was determined by fluorescence microscopy. F. Time-

lapse confocal microscopy of a PyGFP sporozoite (green) in a HepG2/N20-mCherry cell (membranes labeled in red). Images were extracted from Movie S1. A constriction of the parasite is indicated with an arrowhead. Bars, 10 µm. See also Movies S1-2.

Figure 3. PyΔ*plp1* sporozoites accumulate inside non-replicative vacuoles. A-B. HepG2 (A) or HepG2/CD81 (B) cells (5 x 10^4) were incubated with PyGFP or PyΔ*plp1* sporozoites (3 x 10^4) for 10 to 120 minutes, trypsinized, and either directly analyzed by FACS to quantify invaded (GFP-positive) cells (lines), or replated and cultured for an additional 24 hours before quantification of EEFs by fluorescence microscopy (bars). Shown are the mean values (± SD) of triplicate wells. Statistical significance was assessed using two-way ANOVA followed by Bonferroni test. ** p<0.01; *** p<0.001; ns, non significant. C. Electron micrographs of PyΔ*plp1* sporozoites in HepG2 cell. The insets show at higher magnification the parasite plasma membrane (arrow) and the vacuole membrane (arrowheads). The parasite rhoptries are indicated with asterisks. Bars, 1 µm. D. HepG2/N20-mCherry cells (red) were incubated with PyΔ*plp1* sporozoites (green) for 30 min, fixed and labeled with filipin (blue). Bars, 10 µm. E. HepG2/N20-mCherry cells were incubated with PyΔ*plp1* sporozoites for 30 or 120 min before fixation and labeling with filipin, and the presence or absence of a vacuole was determined by fluorescence microscopy. F. Time-lapse confocal microscopy of a PyΔ*plp1* sporozoite (green) in a HepG2/N20-mCherry cell (membranes labeled in red). Images were extracted from Movie S3. Bars, 10 µm. See also Figures S1-3 and Movies S3-7.

Figure 4. Sporozoites form TVs without rhoptry secretion or remodeling of the vacuole membrane. A. HepG2 and HepG2/CD81 were incubated for 2 hours with PyΔ*plp1* sporozoites in the presence of anti-PyCSP antibody or cytochalasin D, and analyzed by FACS to determine the percentage of invaded cells, in comparison to control wells without inhibitors. B. Transgenic PyΔ*plp1*/RON4::mCherry and PyGFP/RON4::mCherry sporozoites were incubated with HepG2 or HepG2/CD81 cells for 60 or 120 min before fixation and filipin

staining. Apical RON4-mCherry fluorescence is indicated with arrowheads. Bars, 10 µm. C. HepG2 and HepG2/CD81 cells were incubated with PyGFP/RON4::mCherry or PyΔ*plp1*/RON4::mCherry sporozoites, labeled with filipin, and the proportion of RON4-depleted sporozoites inside filipin-positive vacuoles was determined by fluorescence microscopy. D. HepG2/N20-mCherry and HepG2/CD81/N20-mCherry cells were incubated with PyΔ*plp1* or PyGFP sporozoites for 30 or 120 min, respectively, fixed, and labeled with filipin. Bars, 10 µm. E-F. HepG2 (E) and HepG2/CD81 (F) cells were incubated for 120 min with PyΔ*plp1* (E) or PyGFP (F) sporozoites, respectively, fixed, and labeled with filipin and either phalloidin-TRITC or anti-Basigin antibodies. Bars, 10 µm. G. Cell cultures processed as in D-F were examined by fluorescence microscopy to determine the proportion of labeled vacuoles among filipin-positive TVs (PyΔ*plp1* sporozoites in HepG2 cells) versus PVs (PyGFP sporozoites in HepG2/CD81 cells). See also Figure S4.

Figure 5. Non-replicative PyΔ*plp1* vacuoles are eliminated by the host cell lysosomes. A. HepG2 or HepG2/CD81 cells (5 x 10^4) were incubated with PyΔ*plp1* sporozoites (3 x 10^4) for 1 to 12 h, and analyzed by FACS to determine the percentage of infected (GFP-positive) cells. B. HepG2 and HepG2/CD81 were incubated with GFP-expressing PyΔ*plp1* sporozoites (green) for 4 h, then labeled with Lysotracker-red and examined by fluorescence microscopy. Bars, 10 µm. C. HepG2 and HepG2/CD81 were incubated with GFP-expressing PyΔ*plp1* sporozoites (green) for 5 h, then fixed and labeled with antibodies against LAMP1 (red) and Hoechst 33342 (blue). Bars, 10 µm. The insets show LAMP1-negative (i and ii) and LAMP1-positive (iii and iv) parasites. D. HepG2/CD81 and HepG2 cells were incubated with PyΔ*plp1* sporozoites for 4 h and labeled as in B and C. The proportion of Lysotracker- or LAMP1-positive parasites was then determined by fluorescence microscopy. At least 100 infected cells were examined per condition. E. Liver sections from BALB/c mice infected with PyGFP or PyΔ*plp1* sporozoites were labeled with antibodies against CSP, UIS4 or LAMP1, and analysed by fluorescence microscopy to determine the proportion of parasites expressing UIS4 and LAMP1 among PyGFP (n = 52) and PyΔ*plp1* (n = 56) parasites. F. HepG2 cells

were treated with chloroquine (CQ) for 12 hours before addition of PyΔ*plp1* sporozoites. The percentage of infected (GFP-positive) cells in treated versus untreated cultures was determined by FACS at 4 and 20 hours post-infection. See also Figure S5.

Figure 6. Blocking lysosomal acidification inhibits sporozoite egress from transient vacuoles. A-B. HepG2/CD81 (A) or HepG2 cells (B) (3×10^4) were pre-treated with bafilomycin A1 or solvent alone (control), then incubated with PyGFP sporozoites (1×10^4) in the presence of rhodamine-conjugated dextran, and analyzed by FACS to determine the percentage of traversed (dextran-positive) cells (lines) and invaded (GFP-positive) cells (bars). Results are expressed as the mean percentage (+/- SD) of triplicate wells. Statistical significance was assessed using two-way ANOVA followed by Bonferroni test (GFP-positive cells: non significant at 15 and 30 min, $p<0.001$ at 60, 90 and 120 min). C-D. HepG2/CD81 or HepG2 cells treated like in A and B were incubated for 24 hours before analysis by FACS (C) and fluorescence microscopy (D), to determine the percentage of infected cells and the proportion of replicative forms (EEFs).

Figure 7. A model of host cell invasion by malaria sporozoites. *Plasmodium* sporozoites invade cells actively inside two types of vacuoles. A. Sporozoites initially enter cells actively inside a transient vacuole (1), without forming a junction, and subsequently egress using PLP1 (2). PLP1-mediated membrane rupture may occur before complete sealing of the primary vacuole (3). PLP1 activity depends on lysosomal acidification, and results in parasite cell traversal and escape from lysosomal degradation. PLP1-deficient parasites cannot breach the vacuole membrane and are trapped inside non-replicative vacuoles, which are eliminated after fusion with the host cell lysosomes (4). B. Sporozoites eventually switch to productive invasion through a moving junction (5), a process that requires the host entry factor CD81 and results in the formation of the PV. Productive invasion is associated with remodeling of the vacuole membrane, precluding its fusion with lysosomes, and leads to parasite liver stage development inside the PV (6). We cannot exclude that some sporozoites

may enter cells through the non-productive invasion pathway and form a junction intracellularly (7), resulting in the remodeling of the initial non-replicative vacuole into a replicative PV.

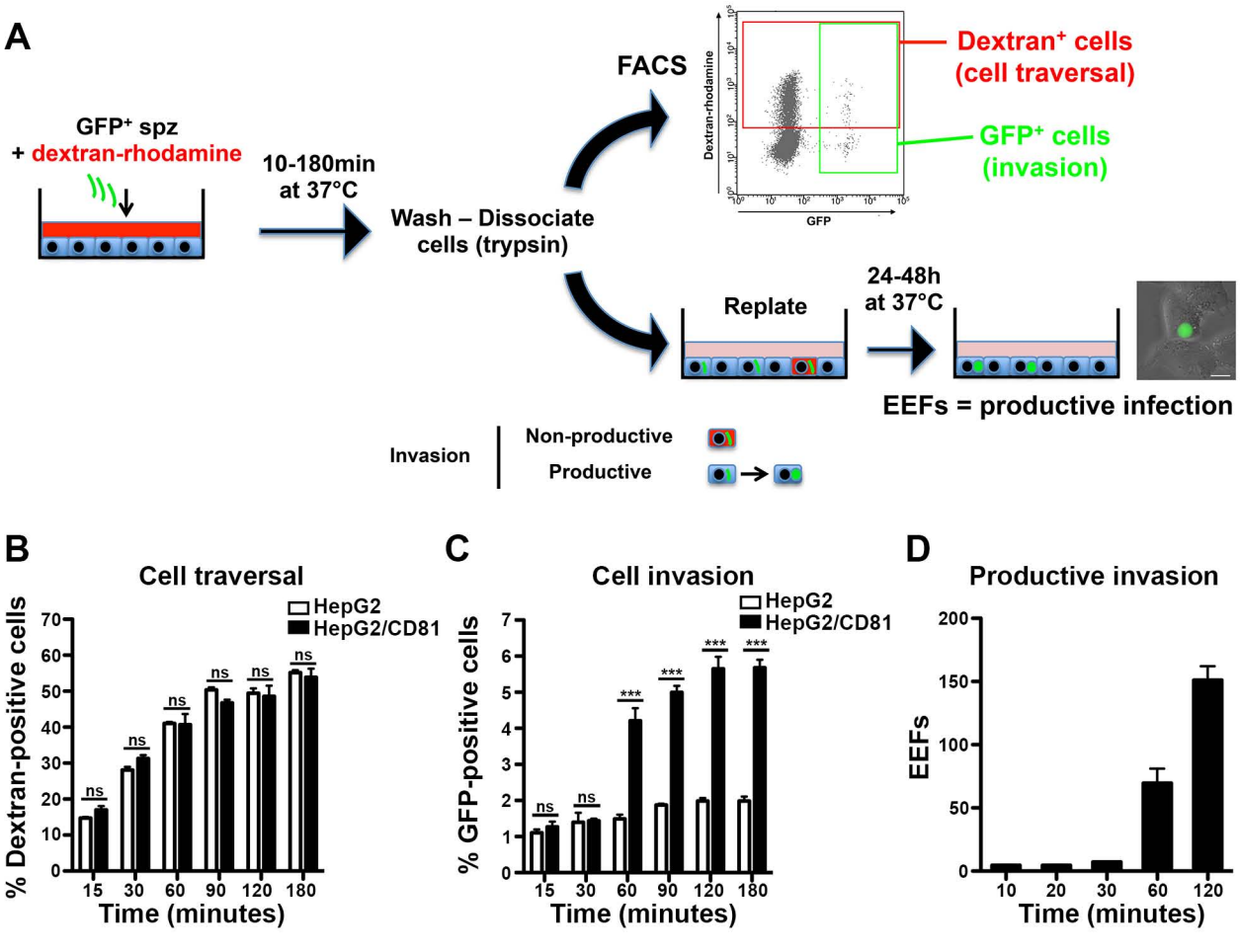
A
GFP+ spz
+ dextran-rhodamine
10-180min
at 37°C
Wash – Dissociate
cells (trypsin)
FACS
Dextran-rhodamine
GFP
Dextran+ cells
(cell traversal)
GFP+ cells
(invasion)
Replate
24-48h
at 37°C
EEFs = productive infection
Invasion
Non-productive
Productive
B
Cell traversal
HepG2
HepG2/CD81
% Dextran-positive cells
Time (minutes)
ns
C
Cell invasion
% GFP-positive cells
***
D
Productive invasion
EEFs

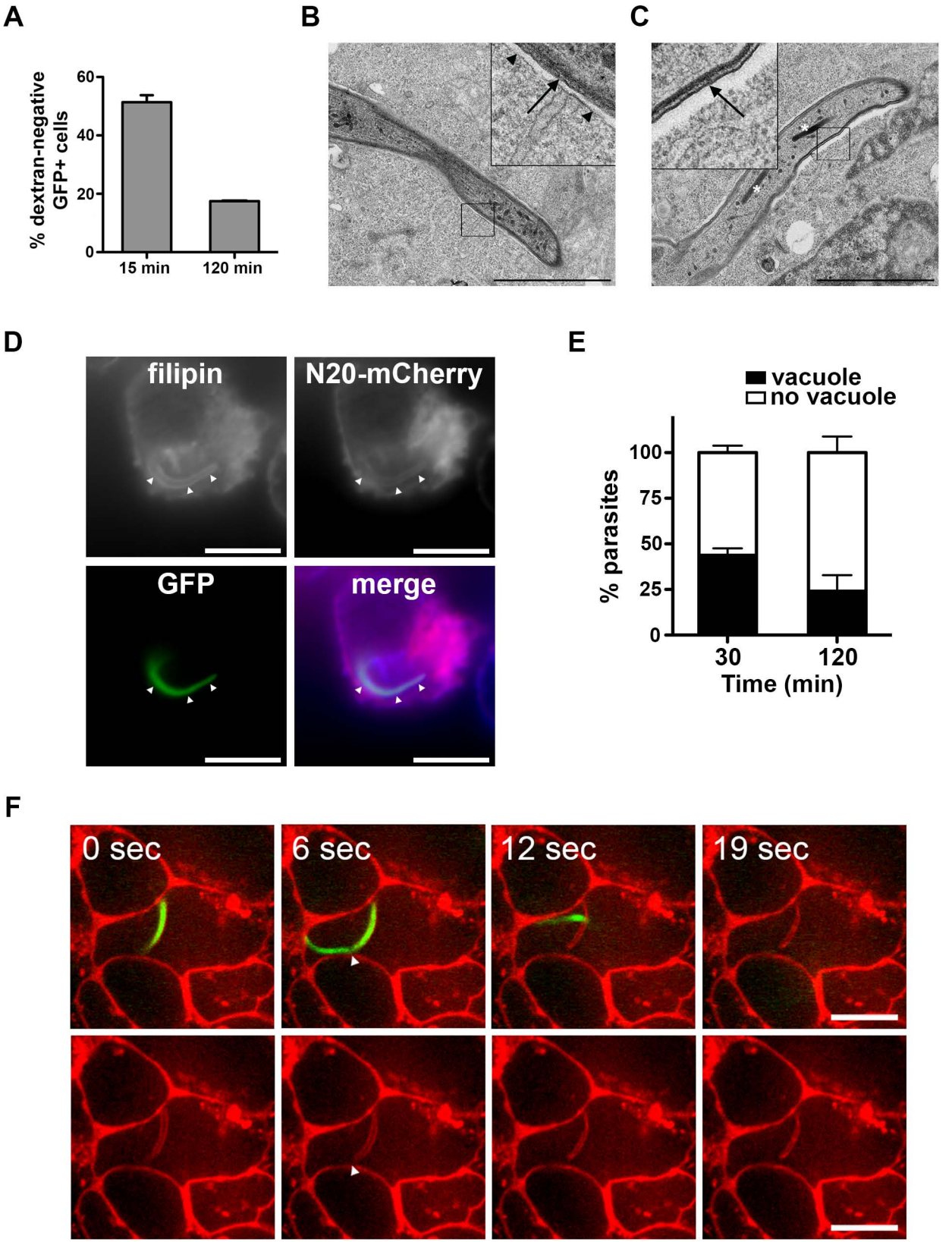
A
% dextran-negative GFP+ cells
60
40
20
0
15 min
120 min
B
C
D
filipin
N20-mCherry
GFP
merge
E
vacuole
no vacuole
% parasites
100
75
50
25
0
30
120
Time (min)
F
0 sec
6 sec
12 sec
19 sec

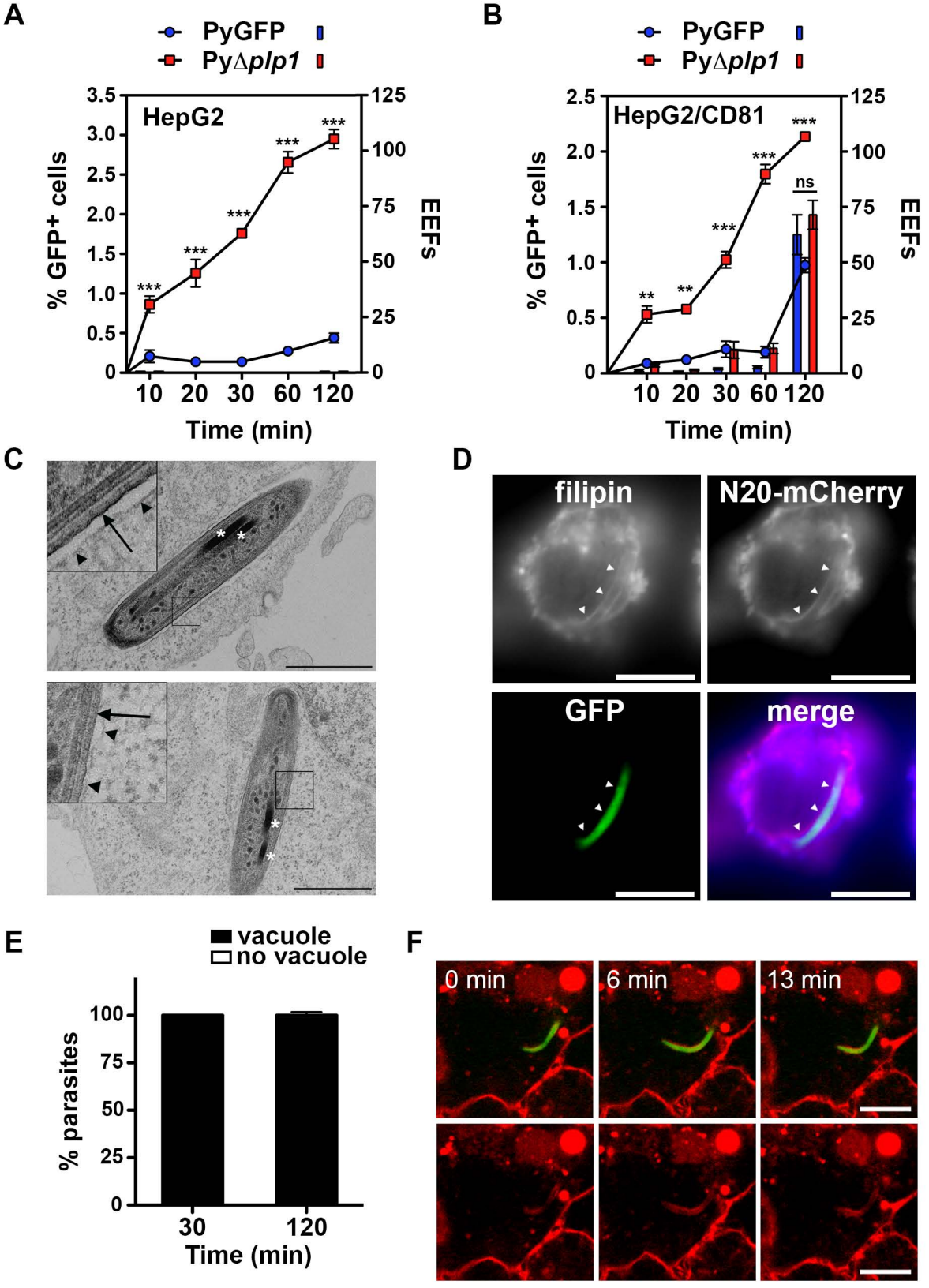
A
PyGFP
PyΔplp1
HepG2
% GFP+ cells
EEFs
Time (min)
B
HepG2/CD81
ns
C
D
filipin
N20-mCherry
GFP
merge
E
vacuole
no vacuole
% parasites
Time (min)
F
0 min
6 min
13 min

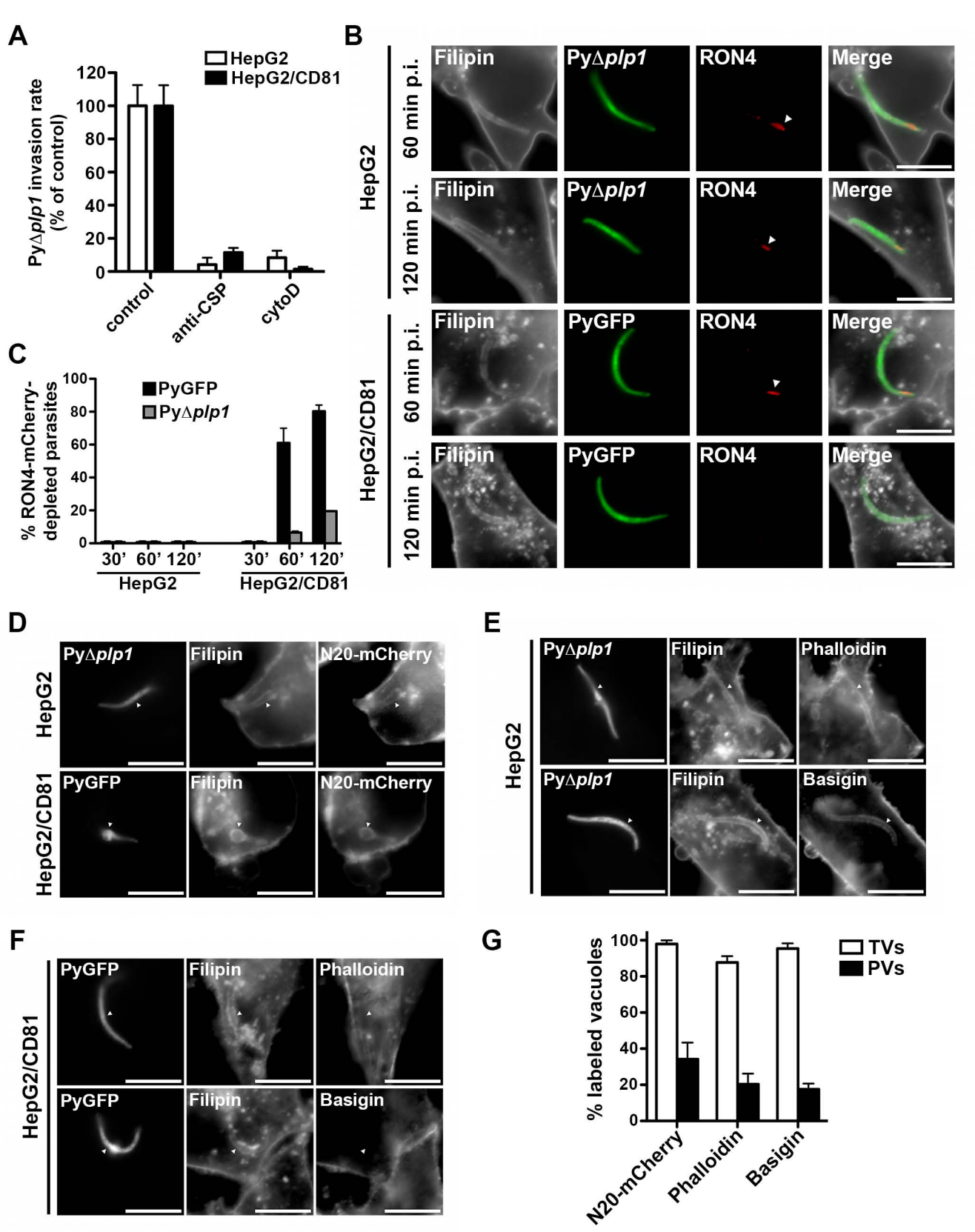
A
HepG2
HepG2/CD81
PyΔplp1 invasion rate (% of control)
120
100
80
60
40
20
0
control
anti-CSP
cytoD
B
HepG2
60 min p.i.
120 min p.i.
HepG2/CD81
Filipin
PyΔplp1
PyGFP
RON4
Merge
C
PyGFP
PyΔplp1
% RON4-mCherry-depleted parasites
100
80
60
40
20
0
30' 60' 120'
30' 60' 120'
HepG2
HepG2/CD81
D
HepG2
HepG2/CD81
PyΔplp1
PyGFP
Filipin
N20-mCherry
E
HepG2
PyΔplp1
Filipin
Phalloidin
Basigin
F
HepG2/CD81
PyGFP
Filipin
Phalloidin
Basigin
G
% labeled vacuoles
100
80
60
40
20
0
TVs
PVs
N20-mCherry
Phalloidin
Basigin

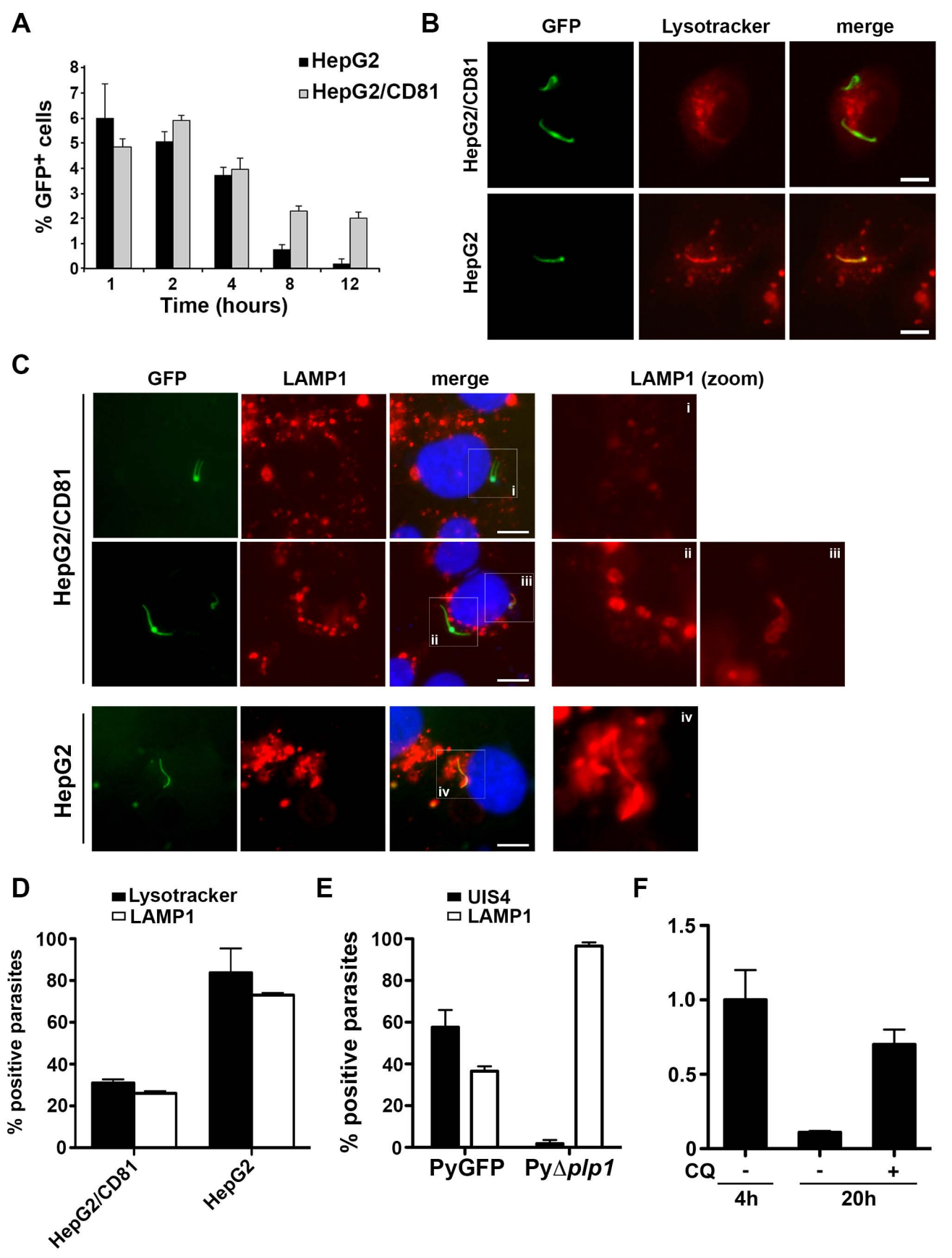
A
HepG2
HepG2/CD81
% GFP+ cells
Time (hours)
B
GFP
Lysotracker
merge
HepG2/CD81
HepG2
C
GFP
LAMP1
merge
LAMP1 (zoom)
HepG2/CD81
HepG2
i
ii
iii
iv
D
Lysotracker
LAMP1
% positive parasites
HepG2/CD81
HepG2
E
UIS4
LAMP1
% positive parasites
PyGFP
PyΔplp1
F
CQ
4h
20h

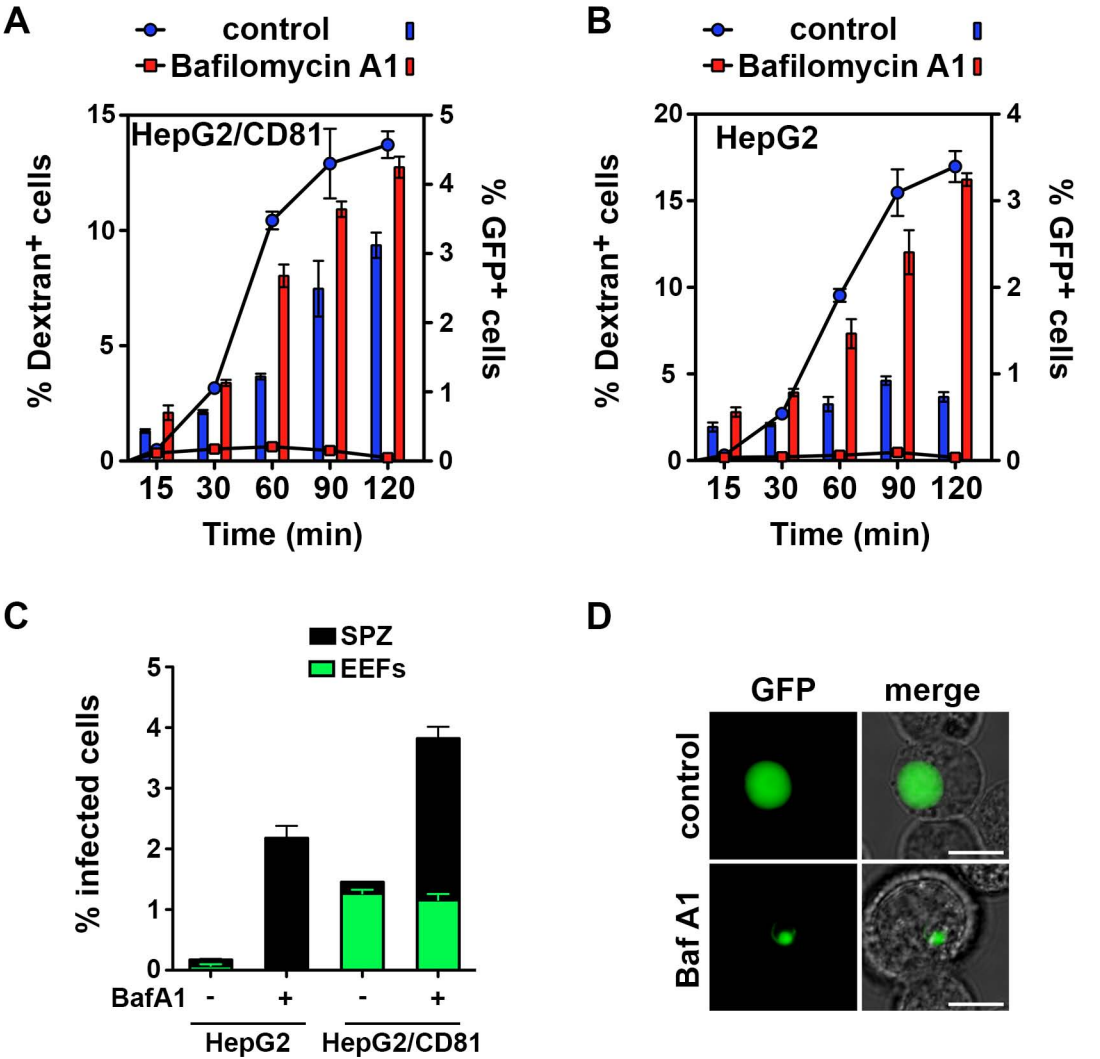
A
control
Bafilomycin A1
HepG2/CD81
% Dextran+ cells
% GFP+ cells
Time (min)
B
control
Bafilomycin A1
HepG2
% Dextran+ cells
% GFP+ cells
Time (min)
C
SPZ
EEFs
% infected cells
BafA1
HepG2
HepG2/CD81
D
GFP
merge
control
Baf A1

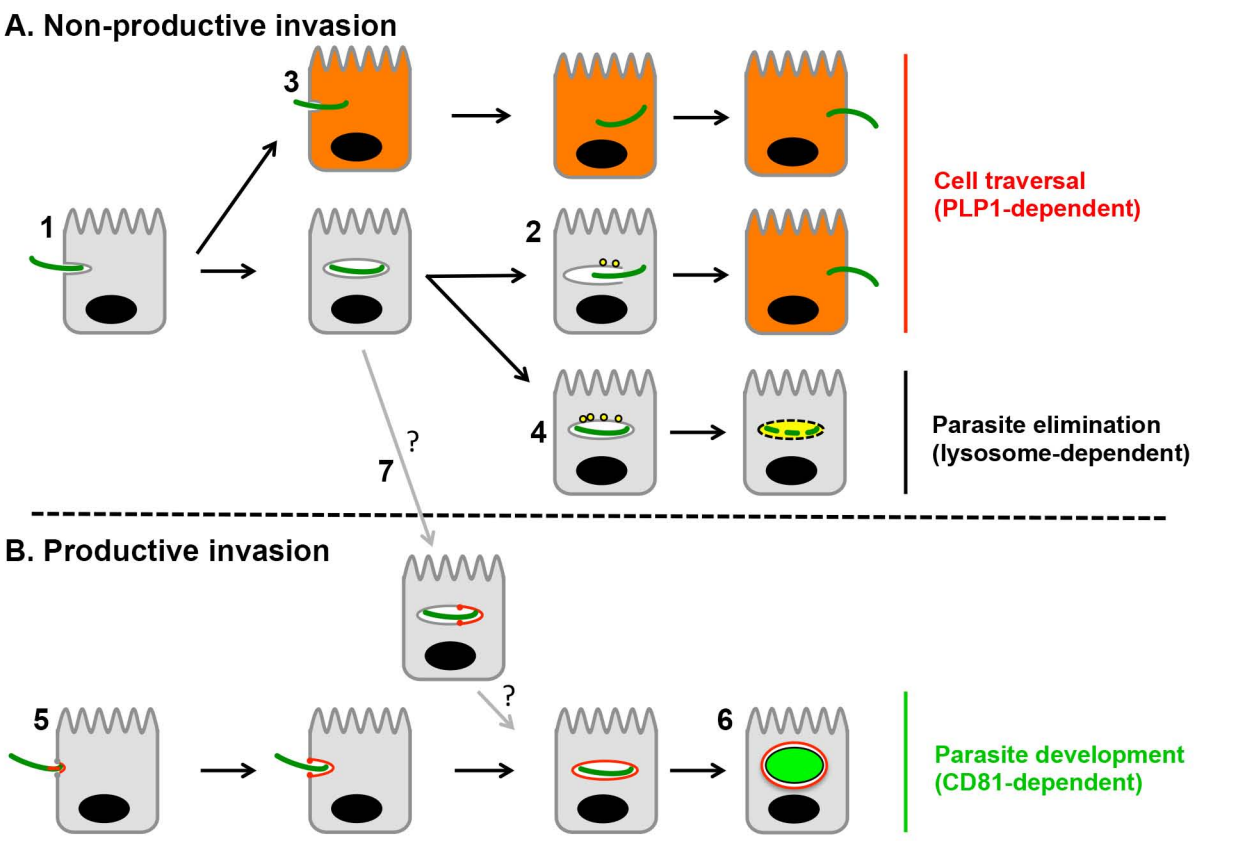
A. Non-productive invasion
1
2
3
4
7
?
Cell traversal
(PLP1-dependent)
Parasite elimination
(lysosome-dependent)
B. Productive invasion
5
6
?
Parasite development
(CD81-dependent)